RSC Advances

This is an *Accepted Manuscript*, which has been through the Royal Society of Chemistry peer review process and has been accepted for publication.

Accepted Manuscripts are published online shortly after acceptance, before technical editing, formatting and proof reading. Using this free service, authors can make their results available to the community, in citable form, before we publish the edited article. This *Accepted Manuscript* will be replaced by the edited, formatted and paginated article as soon as this is available.

You can find more information about *Accepted Manuscripts* in the Information for Authors.

Please note that technical editing may introduce minor changes to the text and/or graphics, which may alter content. The journal's standard Terms & Conditions and the Ethical guidelines still apply. In no event shall the Royal Society of Chemistry be held responsible for any errors or omissions in this *Accepted Manuscript* or any consequences arising from the use of any information it contains.

ROYAL SOCIETY OF CHEMISTRY

www.rsc.org/advances

Cite this: DOI: 10.1039/c0xx00000x

www.rsc.org/xxxxxx

ARTICLE TYPE

Lithium-Coordinating Ionic Conductor for Solid-State Dye-Sensitized Solar Cells

Juan Li and Zhong-Sheng Wang*

Received (in XXX, XXX) Xth XXXXXXXXX 20XX, Accepted Xth XXXXXXXXX 20XX
DOI: 10.1039/b000000x

A new solid-state ionic conductor is synthesized by linking an ether group to the nitrogen-atom of 1,2-dimethylimidazole with an iodide counter anion, and the single crystal structure is determined with X-ray crystallographic analysis. Replacement of the butyl group in 1-butyl-2,3-dimethylimidazolium iodide with an ether group induces significant improvement of conductivity. When the solid ionic conductor is mixed with LiI alone, conductivity enhancement is more remarkable for the ether-containing ionic conductor due to the lithium coordination to the ether oxygen, which is able to avoid the aggregation of lithium cations with iodides and hence improves transport properties of Li^+. Owing to the π-stacking of imidazolium rings for the ether-containing ionic conductor, the increment of ionic conductivity is also more significant upon further doping with I_2. The ether-containing ionic conductor mixed with LiI alone as the solid electrolyte can even make the solid-state dye-sensitized solar cells work. Further doping with iodine achieves power conversion efficiency of 7.1%, which is much higher than that (5.3%) for the alkyl analogue due to the positive shift of conduction band edge of titanium dioxide and suppression of charge recombination caused by the ether group.

Introduction

Dye-sensitized solar cells (DSSCs) employing nanoporous TiO_2 electrode[1] have been attracting considerable attention in industrial and academic fields because of their potential low-cost and high efficiency.[2-5] Although high performance can be achieved with volatile organic liquid electrolytes, solid-state DSSC (ssDSSC) devices mediated with solid-state electrolytes have high application potential due to the stability and safety concerns.[6-10]

Ionic liquids (ILs) have attracted growing interests for use in DSSCs due to their wonderful properties such as negligible vapor pressure, excellent thermal stability, good ionic conductivity and wide electrochemical window.[11,12] 1-methyl-3-propylimidazolium iodide is often used to construct solvent-free DSSCs.[13] To make the DSSC device more stable, a series of solid imidazolium iodides with various functional groups have been developed for use in ssDSSCs.[6,9]

The acidic hydrogen at C-2 position in imidazolium ring usually causes the IL unstable.[14] Replacement of the H atom at C-2 position can improve the stability and meanwhile enhance the melting point significantly.[14] The solid 1,2-dimethyl-3-propylimidazolium iodide is an often used additive in the organic solvent based electrolyte for high-performance organic liquid electrolyte based DSSCs. However, the solid 1,2,3-trialkylimidazolium iodide mixed with iodine and LiI without adding organic solvent cannot make the solid-state DSSCs (ssDSSCs) work efficiently due to the pretty low ionic conductivity.[9] To improve the ionic conductivity of the solid IL, different functional groups have been introduced to the imidazolium ring,[6,9] which results in significant improvement of photovoltaic performance of ssDSSCs.

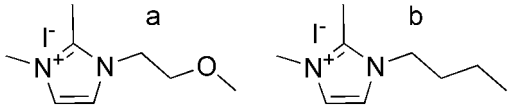

Figure 1. Chemical structures of (a) DOII and (b) DBII

In this study, we synthesized a new ionic conductor, 1,2-dimethyl-3-methoxyethylimidazolium iodide (DOII, Figure 1a), based on 1-butyl-2,3-dimethylimidazolium iodide[15] (DBII, Figure 1b) by replacing one CH_2 unit in the butyl group with an oxygen atom. The aim of introducing an ether group is to induce π-π stacking of imidazolium rings through the H…O hydrogen bonds, which is favourable for efficient charge exchange and can thus increase ionic conductivity. Furthermore, lithium coordination to the ether oxygen can avoid strong aggregates of lithium cations with iodides, thus improving their transport properties, which may influence the conduction band level of titania and the interfacial charge recombination. As compared to DBII, the introduction of an ether group to the imidazolium improved the ionic conductivity significantly for the pure ionic conductors and their mixtures with LiI and with LiI and I_2 as well. When DOII mixed with appropriate amount of LiI and I_2 was employed as the solid electrolyte, the ssDSSC with a metal-free organic dye[16] (FNE29, Figure S1) achieved a power conversion efficiency of 7.1% under AM1.5G full-sun illumination, which was much higher than that (5.3%) with the DBII/LiI/I_2 solid-state electrolyte. Impedance analyses reveal that the ether group

RSC Advances Accepted Manuscript

induces a positive shift of conduction band edge of titanium dioxide and suppression of charge recombination.

Experimental

Materials and Reagents. LiI and I_2 were obtained from Acros. 2-methoxyethanol, 1,2-dimethylimidazole, p-toluenesulfonyl chloride, and 1,1,1-trichloroethane were obtained from Aldrich. Organic solvents were dried according to the standard methods. Transparent conductive glass (F-doped SnO_2, FTO, 14 Ω per square, transmittance of 85%, Nippon Sheet Glass Co., Japan) was used as the substrate for the fabrication of TiO_2 thin film electrodes. The organic dye FNE29 (Figure S1) was prepared according to the reported method.[16]

Fabrication of ssDSSCs. TiO_2 films (12 μm) composed of a 7 μm nanoparticle (25 nm) layer in direct contact with the FTO substrate and a 5 μm light scattering particle (80% 25 nm TiO_2 + 20% 100 nm TiO_2) layer[17] were fabricated with a screen-printing technique. The films were sintered at 500 °C with a rising rate of 10 °C min^{-1} and treated with 0.05 M $TiCl_4$ aqueous solution for 30 min at 70 °C followed by heating at 450 °C for 30 min. Then the films were immersed in the dye solution (0.3 mM in toluene) when the film was about 120 °C for 16 h. The dye-sensitized TiO_2 and the Pt-coated FTO as a counter electrode were separated by a hot-melt Surlyn film (30 μm) and sealed together by pressing them under heat. The methanol solution of the solid electrolyte was injected into the internal space of the cell from the two holes predrilled on the back of the counter electrode and dried on a hot plate with the temperature of 80 °C until the TiO_2 porous film was filled with the solid electrolyte. The devices were further dried in a vacuum oven at 50 °C for 24 h to remove the residue solvent. Finally, the back holes were sealed with a Surlyn film covered with a thin glass slide under heat.

Characterizations. The chemical structures of materials were characterized with ^{1}H-NMR (Varian 400 MHz NMR spectrometer) and ^{13}C-NMR (Varian 500 MHz NMR spectrometer). High-resolution mass spectra (HRMS) were recorded on a MicroTOF II Mass Spectrometer (Bruker Daltonics instrument) with ionization method of electrospray ionization (ESI). The X-ray diffraction data of the DOII single crystal were collected on a Bruker SMART APEX (II)-CCD area detector diffractometer using graphite monochromatic Mo K_α radiation (k = 0.71073 Å) with the ω scan mode 2.59 to 27.90°. Empirical absorption correction was made with multi-scan based on symmetry-related measurements. The structure was solved by a direct method (SHELXLT-97) and refined with full matrix least-squares techniques based on F^2. All non-hydrogen atoms were refined with anisotropic thermal parameters. All computations were carried out using the SHELXL-97 program package. Fourier transition infrared (FT-IR) measurements were performed on Shimadzu IRAffinity-1 FT-IR spectrometer. The ionic conductivity of the solid electrolytes, which were sandwiched between two identical Pt electrodes, was determined with an ac impedance technique on an electrochemical workstation (Zahner CIMPS-1, Germany) with applied bias and ac amplitude were set at 0 V and 10 mV, respectively. The decomposition temperature was determined with Thermo gravimetric (TG) analysis performed on a TG-DTA 2000S system (Mac Sciences Co. Ltd., Yokohama, Japan) at a heating rate of 10 °C min^{-1}. The melting point (m.p.) was derived from Differential Scanning Calorimetry (DSC) performed on a Shimadzu DSC-60A at a heating rate of 5 °C min^{-1}. The film thickness of TiO_2 was measured with a surface profiler (Veeco Dektak 150, USA). The current density-voltage (*J-V*) characteristics of DSSCs were measured by recording the *J-V* curves with a Keithley 2420 source meter under illumination of simulated AM1.5G solar light coming from a solar simulator (Newport, 94023A equipped with a 450 W Xe lamp and an AM1.5G filter). The incident light intensity was calibrated using a standard Si solar cell (Newport 91150). Action spectra of the incident monochromatic photon-to-electron conversion efficiency (IPCE) for the solar cells were obtained with an Oriel-74125 system (Oriel Instruments). The intensity of monochromatic light was measured with a Si detector (Oriel71640). An electrochemical workstation (ZAHNER ZENNIUM CIMPS-1, Germany) was used to perform intensity modulated photovoltage spectroscopy (IMVS) and charge extraction for ssDSSCs under illumination of a green light emitting diode (LED, 532 nm). The intensity-modulated spectra were measured at room temperature with light intensity ranging from 5 to 45 W m^{-2} in modulation frequency ranging from 0.1 Hz to 10 kHz with modulation amplitude less than 5% of the light intensity.

The synthetic route of DOII was illustrated in Scheme S1 in the Supporting Information (SI). DBII was also synthesized to highlight the effect of ether group on the ionic conductivity and the corresponding photovoltaic performance.

Synthesis of 1-chloro-2-methoxyethane. 20.8 g (173 mmol) 2-methoxyethanol and 10.0 g (250 mmol) NaOH dissolved in 50 mL water were charged in a 1 L three-necked flask. Then 36.2 g (190 mmol) 4-methyl-benzenesulfonyl chloride in 50 mL THF was added to the above solution at -5 ^{o}C under the protection of nitrogen. The mixture was stirred at 0 ^{o}C for another 3 h. The resultant mixture was mixed with 200 mL ice water and extracted with CH_2Cl_2 (3×100 mL). The collected organic phase was washed with hydrochloric acid (1 M, 2×250 mL) and brine followed by drying over $MgSO_4$. After the solvent was removed under reduced pressure, the product was obtained as yellowish oil. Yield: 25 g (68%).

Synthesis of 1-iodo-2-methoxyethane. 11.5 g (50 mmol) 1-chloro-2-methoxyethane and 15.0 g NaI (100 mmol) were dissolved in acetone (200 mL) under protection of nitrogen in the dark. The mixture was stirred for 48 h at 25 ^{o}C. After acetone was removed under reduced pressure, CH_2Cl_2 (60 mL) and distilled water (40 mL) were added to extract the organic phase, which was washed with 5% $Na_2S_2O_3$ aqueous solution to remove iodine. Then the organic phase was further washed with saturated $NaHCO_3$ solution (3×50 mL) and distilled water (3×50 mL) followed by drying over Na_2SO_4. After filtration, the product, 1-iodo-2-methoxyethane, was obtained by removing CH_2Cl_2 in the filtrate with rotary evaporator at 50 ^{o}C. ^{1}H-NMR (500 MH_z, DMSO-d_6): δ 2.83~2.79 (t, 2H), 2.55~2.53 (d, 3H), 2.39~2.42 (t, 2H).

Synthesis of 1,2-dimethyl-3-(2-methoxyethyl)imidazolium iodide (DOII, Figure 1a). 96 mg (1 mmol) 1,2-dimethylimidazole and 2.80 g (1.5 mmol) 1-iodo-2-methoxyethane were added to 1,1,1-trichloroethane (10 mL) under protection of nitrogen. The mixture was stirred for 3 h at 40 ^{o}C. After the reaction, the 1,1,1-trichloroethane was decanted and

RSC Advances Accepted Manuscript

This journal is © The Royal Society of Chemistry [year]

the raw product was washed with ether for several times to get DOII as a white powder. Yield: 2.5 g (95%). ^{1}H-NMR (500 MH_Z, DMSO-d6): δ 7.58~7.59 (t, J = 3.3 Hz, 2H), 4.29~4.31 (m, 2H), 3.78~3.79 (d, J = 2.7 Hz, 3H), 3.60~3.63 (t, J = 4.9 Hz, 2H), 3.22 (s, 3H), 2.55~2.56 (d, J = 3.0 Hz, 3H). ^{13}C-NMR (500MH_Z, DMSO-d6): 121.545, 120.574, 101.311, 69.191, 57.546, 46.791, 34.134, 8.770. The decomposition temperature: 310 °C; m.p. 83 °C. HRMS (ESI. *m*/*z*): calcd for $C_8H_{15}ON_2^+$, 155.1184; found 155.1208.

Synthesis of 1,2-dimethyl-3-butylimidazolium iodide (DBII, Figure 1b). DBII was prepared according to the reported method.[15] 96 mg (1 mmol) 1,2-dimethyl imidazole and 2.76 g (1.5 mmol) 1-butyliodide were charged in 1,1,1-trichloro-ethane (10 mL) under protection of nitrogen. The mixture was stirred for 3 h at 40 °C. After the reaction, the 1,1,1-trichloroethane was decanted and the raw product was washed with ether for several times to get a white powder as the final product. Yield: 2.5 g (95%). ^{1}H-NMR (500 MH_Z, DMSO-d_6): δ7.62~7.61 (d, 2H), 7.46~7.45 (d, 3H), 4.2~4.18 (t, 2H), 4.01 (s, 3H), 2.84 (s, 3H), 1.82~1.81 (m, 2H), 1.42~1.41 (m, 2H), 0.98~0.97 (t, 3H). m.p. 105 °C, the decomposition temperature 298 °C.

Results and Discussion

A colourless lamellar crystal was obtained by slow evaporation of a solution in methanol at room temperature. Single-crystal X-ray analysis reveals that the DOII salt crystallizes in monoclinic space group (CCDC 948215) with crystallographic details listed in Table S1. To emphasize the function of ether group, the crystal structure of DBII (Figure S2) was downloaded from the Cambridge Crystallographic Data Centre (CCDC 634384) for comparison. Figure 2 shows the single-crystal structure of DOII. In the single crystal structure, there is one cation for DOII (Figure 2) while there are two cations for DBII (Figure S2). The ether oxygen does not affect the space group but reduces the cell lengths. The cell volume is reduced by more than 2-fold from butyl to ether substitution. In the DBII crystal, there is one H…I hydrogen bond with a distance of 2.915 Å. For DOII, there are three H…O hydrogen bonds while the H…I hydrogen bonding is absent. This indicates that the ether oxygen competes with the iodide for the hydrogen bonding.

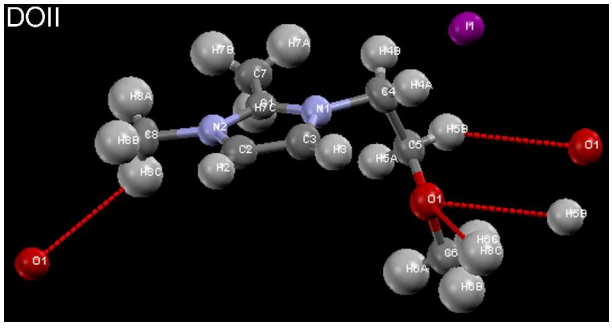

Figure 2. Single-crystal structure of DOII along with the hydrogen bonds

The packing structures of DOII and DBII are shown in Figure 3 and Figure S3, respectively. DOII and DBII exhibit different packing structures because of their different hydrogen bonds between neighbouring molecules. Dimers of DOII are formed by means of two H5B…O (2.880 Å, Figure 2) hydrogen bonds between the two adjacent molecules. The crystal structure of DOII is expanded *via* linking the dimers with H8c…O (2.957 Å, Figure 2) hydrogen bonds, forming a lamellar structure. The centroid-centroid distance is 4.4 Å for DOII and 5.9 Å for DBII. As π-π interaction exists when the centroid-centroid distance is smaller than 4.6 Å,[18] it is inferred that the imidazolium rings are π-stacked for DOII while they are not for DBII.

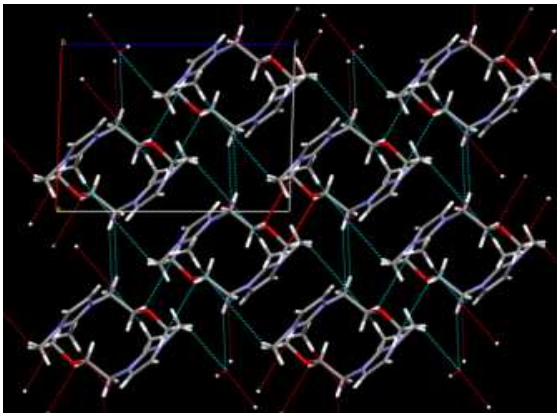

Figure 3. Packing structure of DOII viewed along the *b* axis

The different packing structure caused by different functional groups in the imidazolium ring is expected to influence the ionic conductivity. The ionic conductivities at room temperature of the pure ionic conductors and their mixtures doped with LiI (molar ratio of ionic conductor/LiI = 2/1) and further doped with iodine (molar ratio of ionic conductor/LiI/I_2 = 2/1/0.2) were measured with EIS using dummy cells, in which the solid electrolytes were sandwiched between two identical Pt electrodes. Figure S4 illustrates the EIS Nyquist plots of the above solid electrolytes. The left semicircle is attributed to the charge transfer resistance (R_{ct}) at the electrode/electrolyte interface while the right semicircle is attributed to the resistance of solid electrolyte (R_{EL}).[19] Fitting the impedance spectra with the equivalent circuit (inset of Figure S4) using the Z-view software gives R_{ct} and Z_{EL}. The ionic conductivity (σ) is calculated with $\sigma = d/(Z_{EL} \times S)$, where d is the thickness and S is the area of the solid electrolyte. Interestingly, replacement of one CH_2 unit in the butyl group of DBII with an oxygen atom can increase the conductivity by more than 3-fold from 0.017 to 0.055 mS cm^{-1} (Figure 4). Structural difference is likely the main reason for the different ionic conductivities. The ether bond diminishes the van der Waals interactions among the side chains,[20] making the organic cations move more freely and thus resulting in higher ionic conductivity for DOII. As the ionic conductivity is low, the R_{ct} is high: 34 Ω for DOII and 110 Ω for DBII.

RSC Advances Accepted Manuscript

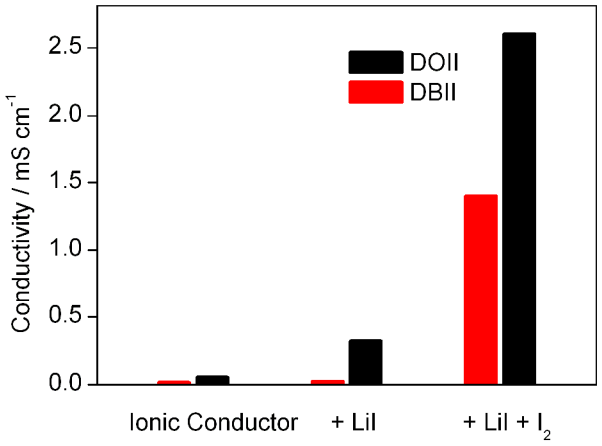

Figure 4. Ionic conductivities for various solid electrolytes

When LiI is doped into the solid ionic conductors (ionic conductor/LiI = 2/1), the ionic conductivity for both DOII and DBII increased due to the increased number of charged species. However, the increment of conductivity is quite different for DOII and DBII. Upon doping of LiI into the solid ionic conductor, the conductivity of DBII increased slightly from 0.017 to 0.024 mS cm^{-1} while the conductivity of DOII increased significantly from 0.055 to 0.32 mS cm^{-1} (Figure 4). The R_{ct} decreased to 5 Ω for DOII and 35 Ω for DBII due to the enhanced conductivity upon LiI doping. The increase in conductivity for DOII is more pronounced than that for DBII upon LiI doping. As reported in the literature,[20] the strong interaction of Li^+ with iodide can diminish the transport properties of Li^+ ions, and therefore, the increase in ionic conductivity is not notable. As the ether oxygen in DOII can, however, compete with iodide anions for Li^+, the mobility of lithium ions is expected to increase, resulting in significant improvement of conductivity.[20] It is thus likely that the Li^+ ion dominates the contribution to increase the conductivity for the mixture of ionic conductor and LiI.

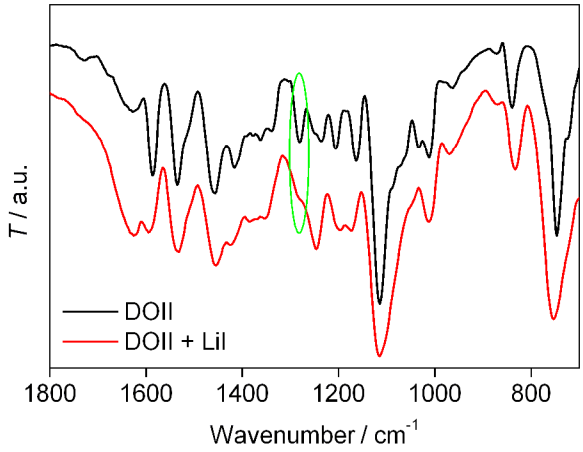

Figure 5. IR spectra of DOII and DOII/LiI

Figure 5 shows the FTIR spectra of DOII and DOII/LiI mixture. The peak at 1282 cm^{-1} attributed to the asymmetric stretching vibration of C-O-C bond[21] is clearly observed for DOII, but it diminishes for the DOII/LiI mixture. This is due to the coordination of ether oxygen to Li^+ ions. Therefore, the ether oxygen atom can avoid aggregation of Li^+ with iodide anions and thus increases the number of charged species, resulting in enhanced conductivity.[20]

Upon further doping with iodine (ionic conductor/LiI/I_2 = 2/1/0.2), the conductivity increases to 2.6 mS cm^{-1} and 1.4 mS cm^{-1} for DOII and DBII, respectively, as shown in Figure 4. The remarkable increase in ionic conductivity stems from the formation of polyiodides such as I_3^- ions by means of reaction between iodide and iodine. The formation of polyiodides facilitates the charge transfer along the polyiodides chain via the Grotthus-type exchange mechanism,[22-24] which is responsible for the remarkable enhancement of conductivity. The increment of ionic conductivity arising from the Grotthus charge exchange for DOII is larger than that for DBII upon iodine doping. This is attributed to the π-π stacking in DOII, which is advantageous to efficient Grotthus bond exchange due to the reduced distance between the iodide/polyiodide species. In this case, the R_{ct} further decreased to 2 Ω for DOII and 3 Ω for DBII.

It is seen from Figure 4 that DOII exhibits higher conductivity than DBII. The ionic conductivity increases from pure ionic conductor to LiI doping and then to LiI + I_2 doping for both compounds. For each doping, the increment of conductivity for DOII is larger than that for DBII. Evidently, the ether oxygen contributes positively to the increased ionic conductivity. As a consequence, DOII based solid electrolytes show higher conductivity than DBII based electrolytes in either pure phase or mixture.

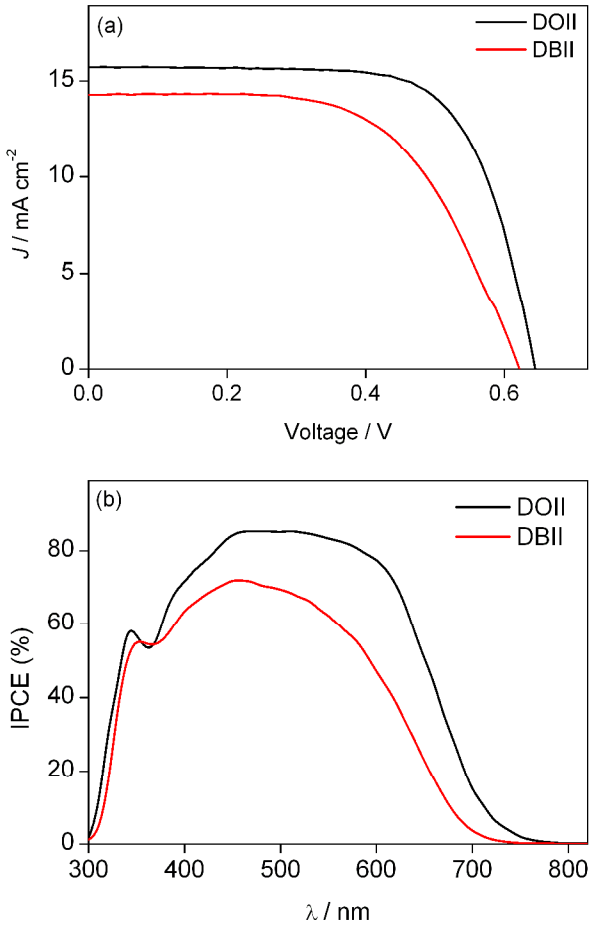

Figure 6. (a) *J-V* curves and (b) IPCE spectra for ssDSSCs with DOII or DBII solid electrolytes (DOII/LiI/I_2 = 2/1/0.2, DBII/LiI/I_2 = 2/1/0.2)

RSC Advances Accepted Manuscript

This journal is © The Royal Society of Chemistry [year]

Next, we apply these solid ionic conductors and their mixtures as solid electrolytes for ssDSSCs. It is noted that the used electrolytes are solid state under the operating conditions of solar cells. Since the pure ionic conductors have pretty low conductivity and high R_{ct} values, they cannot make the ssDSSC work without any doping. Upon doping with LiI, the ssDSSC with DOII works with a power conversion efficiency (η) of 3.4% because of the increased conductivity and decreased R_{ct}. However, the ssDSSC with DBII+LI does not work because the conductivity is still low and the R_{ct} is still high. These results indicate that the ssDSSC can work only when the ionic conductivity is larger than a threshold value. Upon further doping with iodine, it is expected to observe improved performance due to the enhanced conductivity. Figure 6a displays the *J-V* curves of ssDSSCs recorded under simulated AM1.5G solar light (100 mW cm^{-2}). The ssDSSC based on DBII/I_2/LiI produced a short circuit photocurrent (J_{sc}) of 14.26 mA cm^{-2}, an open-circuit photovoltage (V_{oc}) of 622 mV, and a fill factor (*FF*) of 0.60, corresponding to η of 5.3%. The ssDSSC based on DOII/I_2/LiI produced a J_{sc} of 15.73 mA cm^{-2}, V_{oc} of 642 mV, and *FF* of 0.70, corresponding to a PCE of 7.1%. The replacement of an oxygen atom in the butyl group increases the J_{sc} and FF significantly, resulting in much improved PCE from 5.3% to 7.1%. The higher FF for DOII is the result of its higher conductivity and lower R_{ct} (left arc in Figure S4c). The higher J_{sc} for DOII is attributed to its greater conductivity and higher electron injection yield to be discussed below. The IPCE action spectra are shown in Figure 6b. The maximum IPCE value is higher than 80% for DOII while it is about 65% for DBII. The difference of IPCE values accounts for the different J_{sc} values.

As the conduction band (CB) edge of TiO_2 may shift with the electrolyte,[25] the relative position of CB, which can influence J_{sc}, V_{oc}, and *PCE*, has been investigated. Figure 7 shows the plot of charge density (Q) at open circuit against open-circuit photovoltage under LED light with various intensities. For both electrolytes, the V_{oc} increases with the logarithm of charge density, and the slope is almost the same (120 mV). As compared to the DBII/LiI/I_2 electrolyte, the DOII/LiI/I_2 electrolyte shows lower CB edge by about 50 mV, as seen from Figure 7. The interaction of ether oxygen with Li^+ ions diminishes the strong coulombic interaction of Li^+ ions with iodides, which improves the transport properties of Li^+ ions.[20] It is thus reasonable that more Li^+ ions for the DOII case can be adsorbed on the TiO_2 surface than for the DBII case, which accounts for the relatively lower CB edge for DOII. As compared to DBII, the positive shift of CB for DOII is beneficial for higher electron injection yield, which in combination with the higher ionic conductivity is responsible for the observed higher J_{sc} and IPCE for DOII. However, the positive shift of CB should lead to a decrease in V_{oc},[25] contrasting to the observation that the device with DOII shows slightly higher V_{oc} than that with DBII. This suggests that charge recombination rate in the two devices should be different.

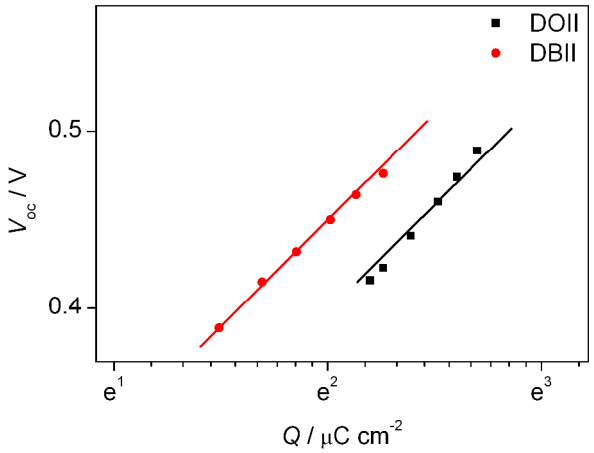

Figure 7. Open-circuit photovoltage as a function of charge density

Figure 8 shows the relationship between electron lifetime and charge density obtained from charge extraction. Electron lifetime is enhanced by about 4-fold from DBII to DOII at the same charge density. This indicates that charge recombination between electrons and triiodide is retarded remarkably when the electrolyte is changed from DBII to DOII. The slower charge recombination for the DOII case is caused by more Li^+ ions adsorbed on the TiO_2 surface.[26] The increase in electron lifetime brings about more electrons stored in TiO_2, resulting in improvement of V_{oc} from DBII to DOII. The charge densities, which depend on the photo-injected electron density and electron lifetime at open-circuit, are measured of 8 and 14 μC cm^{-2} under the same LED light (30 W m^{-2}, 532 nm) for DBII and DOII, respectively. It is derived from Figure 7 that V_{oc} gain solely arising from the increased charge density is about 67 mV. Therefore, the collective effects of the positively shifted CB edge (50 mV) and the increased charge density contribute to an increase in V_{oc} by 17 mV, which is in good agreement with the observed increase in V_{oc}. The V_{oc} gain originating from the increased electron lifetime compensates for the V_{oc} loss arising from the positive shift of conduction band edge, resulting in slightly higher photovoltage.[27]

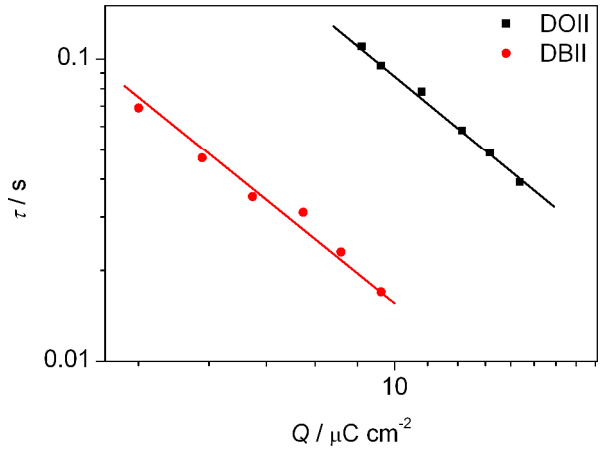

Figure 8. Electron lifetime as a function of charge density at open circuit

The stability for the ssDSSC based on the DOII based solid electrolyte was recorded over a period of 1000 h under one-sun soaking. As shown in Figure 9, at the beginning stage below 200

RSC Advances Accepted Manuscript

h, J_{sc} increases, V_{oc} and FF decreases with time due to the aging effect, resulting an increase in PCE with time up to 200 h. After device aging for 200 h, the device performance becomes steady; all parameters remain almost constant with time. These data indicates that the ssDSSC with DOII based solid electrolyte and an organic dye is long-term stable under one-sun soaking.

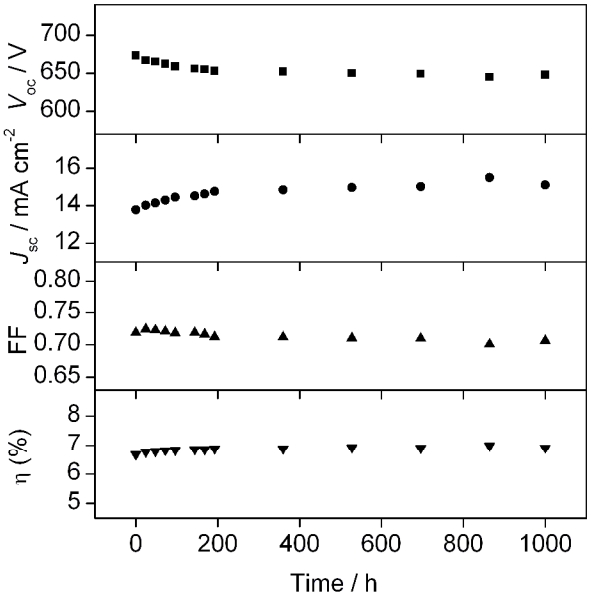

Figure 9. The long-term stability of ssDSSC with DOII based solid electrolyte

Conclusions

In summary, an ether-functionalized imidazolium iodide conductor was designed and synthesized for use as a solid-state electrolyte in ssDSSCs. When one methane unit in the butyl group of DBII was replaced with an oxygen atom, the packing structure changes greatly due to the presence of H…O hydrogen bonds, resulting in different ionic conductivity. Upon doping with LiI, the ionic conductivity was improved more significantly for DOII than for DBII, as the ether oxygen diminished the interaction between Li^+ and iodide, which raised the number of charged species. Further doping with iodine, the increment of conductivity was also more remarkable for DOII than for DBII because of the formation of π-stacking in the former. The presence of ether bond was found to shift the CB edge of TiO_2 positively and to retard charge recombination. As compared to DBII, the DOII produced higher J_{sc}, due to the higher ionic conductivity and higher electron injection yield caused by the lower CB edge, and comparable V_{oc}, due to the opposite effects of CB edge shift and charge recombination suppression. A power conversion efficiency of 7.1% was obtained for an organic dye based ssDSSC with DOII/I_2/LiI as the solid electrolyte, which was much higher than the efficiency of 5.3% for the DBII case at the same conditions. In addition, a long-term stability test demonstrated that the ssDSSC device was stable under one-sun soaking.

Acknowledgment

This work was financially supported by the National Basic Research Program (No. 2011CB933302) of China and STCSM (12JC1401500).

Notes and references

Department of Chemistry, iChEM (Collaborative Innovation Centre of Chemistry for Energy Materials), Lab of Advanced Materials, Fudan University, 2205 Songhu Road, Shanghai 200438, P. R. China
* Corresponding author. E-mail: zs.wang@fudan.edu.cn
§ Electronic Supplementary Information (ESI) available: See DOI: 10.1039/b000000x/

1. M. Grätzel, *Nature* 2001, **414**, 338-334.
2. Y. Bai, Y. Cao, J. Zhang, M. Wang, R. Li, P. Wang, S. M. Zakeeruddin, M. Grätzel, *Nat. Mater*. 2008, **7**, 626-630.
3. H. N. Tian, X. A. Jiang, Z. Yu, L. Kloo, A. Hagfeldt, L. C. Sun, *Angew. Chem., Int. Ed*. 2010, **49**, 7328-7331.
4. A. Hagfeldt, G. Boschloo, L. C. Sun, L. Kloo, H. Pettersson, *Chem. Rev*. 2010, **110**, 6595-6663.
5. F. Gong, H. Wang, X. Xu, G. Zhou, Z. S. Wang, *J. Am. Chem. Soc.* 2012, **134**, 10953-10958.
6. H. Wang, X. Zhang, F. Gong, G. Zhou, Z.-S. Wang, *Adv. Mater*. 2011, **24**, 121-124.
7. I. Chung, B. Lee, J. He, R. P. H. Chang, M. G. Kanatzidis, *Nature*, 2012, **485**, 486-489.
8. J. Wu, S. Hao, Z. Lan, J. Lin, M. Huang, Y. Huang, P. Li, S. Yin, T. Sato, *J. Am. Chem. Soc*. 2008, **130**, 11568-11569.
9. H. Wang, H. Li, B. Xue, Z. Wang, Q. Meng, L. Chen, *J. Am. Chem. Soc.* 2005, **127**, 6394-6401.
10. N. Yamanaka, R. Kawano, W. Kubo, T. Kitamura, Y. Wada, M. Watanabe, S. Yanagida, *Chem. Commun*. 2005, **6**, 740-742.
11. J. Le Bideau, L. Viau, A. Vioux, *Chem. Soc. Rev.* 2011, **40**, 907-925.
12. F. Mazille, Z. Fei, D. Kuang, D. Zhao, S. M. Zakeeruddin, M. Grätzel, P. J. Dyson, *Inorg. Chem*. 2006, **45**, 1585-1590.
13. D. Kuang, P. Wang, S. Ito, S. M. Zakeeruddin, M. Grätzel, *J. Am. Chem. Soc*. 2006, **128**, 7732-7733.
14. E. I. Izgorodina, R. Maganti, V. Armel, P. M. Dean, J. M. Pringle, K. R. Seddon, D. R. MacFarlane, *J. Phys. Chem. B* 2011, **115**, 14688-14697.
15. J. Kutuniva, R. Oilunkaniemi, R. S. Laitinen, J. Asikkala, J. Kärkkäinen, M. K. *Z.* Lajunen, *Naturforsch*. 2007, **62b**, 868-870.
16. Y. Li, H. Wang, Q. Y. Feng, G. Zhou, Z.-S. Wang, *Energy Environ. Sci.* 2013, **6**, 2156-2165.
17. Z.-S. Wang, H. Kawauchi, T. Kashima, H. Arakawa, *Coord. Chem. Rev*. 2004, **248**, 1381-1389.
18. C. Janiak, *J. Chem. Soc.-Dalton Trans.* 2000, **21**, 3885-3896.
19. A. Hanch, A. Georg, *Electrochim. Acta* 2001, **46**, 3457-3466.
20. M. J. Monteiro, F. F. Camilo, M. C. C. Ribeiro, R. M. Torresi, *J. Phys. Chem. B* 2010, **114**, 12488-12494.
21. Z. Fei, W. H. Ang, D. Zhao, R. Scopelliti, E. E. Zvereva, S. A. Katsyuba, P. J. Dyson, *J. Phys. Chem. B*. 2007, **111**, 10095-10108.
22. F. C. Küpper, M. C. Feiters, B. Olofsson, T. Kaiho, S. Yanagida, M. B. Zimmermann, L. J. Carpenter, G. W. Luther, Z. L. Lu, M. Jonsson, L. Kloo, *Angew. Chem., Int. Ed*. 2011, **50**, 11598-11620.
23. V. K. Thorsmølle, G. Rothenberger, D. Topgaard, J. C. Brauer, D. B. Kuang, S. M. Zakeeruddin, B. Lindman, M. Grätzel, J. E. Moser, *ChemPhysChem* 2011, **12**, 145-149.
24. R. Kawano, M. Watanabe, *Chem. Commun*. 2003, **3**, 330-331.
25. G. Schlichthörl, S. Y. Huang, J. Sprague, A. J. Frank, *J. Phys. Chem. B* 1997, **101**, 8141-8155.
26. N. Kopidakis, K. D. Benkstein, J. Lagemaat, A. J. Frank, *J. Phys. Chem. B* 2003, **107**, 11307-11315.
27. Z.-S. Wang, G. Zhou, *J. Phys. Chem. B* 2009, **113**, 15417-15421.

RSC Advances Accepted Manuscript

This journal is © The Royal Society of Chemistry [year]